SUPPLEMENTARY FIGURE LEGENDS

Figure S1: Multi-scale association of GC and ToR. A) Multi-scale analysis of standard deviation of GC content. Shown is the standard deviation of GC content (Y axis) in sets of non-overlapping bin sizes at different size scales (X axis). Also shown are the standard deviation expected for bins of similar sizes, assuming nucleotides are randomly sampled according to a unique GC content parameter (gray curves). **B-D) Multi-scale visualization of GC content and ToR.** Shown are domainograms of GC content and ToR, similarly to figure 1B-C but for different genomic coordinates.

Figure S2: Multi-scale analysis of GC content and repressive marks. A) Multi-scale visualization of nuclear lamina proximity. Similarly to figure 1B-D and for the same genomic positions, shown is a domainogram of ChIP-seq signal of laminB1 (red - low, blue - high) of Tig3 cells(1). **B) Correlation of laminB1 and GC content at different scales.** Shown are spearman correlation scores between GC content and laminB1 (y-axis) at different bin sizes (x-axis). **C) Multi-scale visualization of H3K27me3.** Similarly to figure 1B-D, S2A and for the same genomic coordinates, shown is a domainogram of ChIP-seq signal of H3K27me3 of HeLa cells (red - low, blue – high). **D) Correlation of H3K27me3 and GC content at different scales.** Shown are spearman correlation scores between GC content and H3K27me3 (y-axis) at different bin sizes (x-axis). **E) Multi-scale visualization of nucleosome occupancy.** Similarly to figure 1B-D, S2A,S2C and for the same genomic coordinates, shown is a domainogram of MNAse-seq signal of lymphoblastoid cells(2) (blue - low, red – high). **F) Correlation of nucleosome occupancy and GC content at different scales.** Shown are spearman correlation scores between GC content and nucleosome occupancy (y-axis) at different bin sizes (x-axis).

Figure S3: Muti-scale correlation analysis of functional elements density and GC or ToR. A-C) Multi-scale visualization of functional elements density (similar to Figure 1E, at three additional genomic locations. D) Multi-scale analysis of standard deviation of functional elements density. Shown are the observed standard deviation of average functional elements density and the expected standard deviation for binomially distributed functional density (y-axis, black and gray curves) at different bin sizes (x-axis). **E) Correlation of functional elements density and ToR at 100kbps scale.** This density plot depicts functional elements density (y-axis) against ToR (x-axis) averaged over 100kbs bins. **F) Multi-**

scale correlation analysis of functional elements density and ToR. Shown is spearman correlation of functional elements density and ToR (y-axis) averaged over different bin sizes (x-axis). **G) Multi-scale visualization of GC content at functional sites and functionally masked regions.** Domainograms of GC content across a section of chromosome 3 as in figure 1A but only for functionally annotated regions (top) or with masking functionally annotated regions (bottom). **H) Masked GC vs. ToR stratified by nucleosome occupancy.** Shown is the masked GC content at 7 bins of nucleosome occupancy (x-axis) at early and late ToR (red and black curves respectively). **I) Multi-scale correlation analysis of functional elements density and masked/genomic GC content.** Shown is spearman correlation between functional elements density and genomic (black curve) and masked genomic (red curve) GC-content (y-axis) averaged over different bin sizes (x-axis).

Figure S4: Chromosomal domains, GC and ToR. A) Domain size distribution of IMR90 cells. Domain size histogram of re-analyzed Hi-C data from IMR90 cells (3). **B) Visualization of Hi-C maps and projected GC content/ToR profiles.** Chromatin interaction intensity matrix around border of six late replicating domains are shown (bottom, strong interaction levels –orange, weak interaction levels - blue) with linear profiles of functional elements density, ToR, GC content and inferred evolutionary rates of GC gain and GC loss that correspond to the same genomic section (top).

Figure S5. Spatial profiles of GC content and ToR around borders of repressive domains. Shown are averaged ToR **(A)**, GC content **(B)**, masked GC content **(C)**, density of functional elements **(D)**, laminB1 **(E)**, and Hi-C scaling factor **(F)** (y-axis), binned by the distance (x-axis) to borders between active (left) and repressed (right) Hi-C domains (IMR90).

Figure S6: GC content changes gradually with the ToR along TTRs, but not along CTRs which have constant ToR. ToR maps were analyzed using ARTO(4), and replication activity type of every genomic region was determined as CTR (Constant Time Regions) and TTR (temporal Transition Regions). All TTRs (beside the 5% shortest segments) (A-B) and all CTRs (beside segment >2Mb) (C-D) were divided(4) into 3 groups (Early, Middle and Late; each spanning third of the cell cycle) according to the ToR at the earliest border of the segment. For each ToR group, segments were aligned from their borders and all data points were grouped into five equally spaced locations. The average GC content (A and C) and ToR (B and D) of the groups is shown.

Figure S7: GC and ToR profiles around origins of replication. Shown are genomic/masked genomic GC (black and red curves of upper row) and ToR of HeLa cells (black curve, lower row) against the distance from CTCF peaks (A) ORC1 peaks (B), Bubble-seq peaks (C), and DHS (D) which are stratified by three bins of ToR (inner columns).

Figure S8: Deamination rate and SNP analysis of early and late replicating regions. A) Shown is CpG deamination rate (y-axis) vs. CpG content (x-axis, number of CpGs in 500bp window) in early replicating regions (red curves) and late replicating regions (black curves) for whole genome (left) and masked genome (right). **B) GC substitution bias vs. ToR in constitutive ToR regions.** Similarly to figure 3C but only for genomic regions with constitutive ToR(5), shown is the rate of GC gaining substitutions divided by the sum of rates of GC gaining and GC losing substitutions for intergenic (left) or functionally masked (right) regions. **C-G)** As in Fig 3D-F Shown are frequency of low frequency GC gaining alleles (red curve) and GC losing alleles (blue curves) for the whole intergenic genome (left) and for functionally masked regions vs. ToR in GM06990 **(C)**, BJ **(D)**, K562 **(E)**, TL010**(F)** H0287 **(G)** cell lines, primary fibroblasts (FFT) **(G)** and for molt cells when restricting for variable ToR regions(5)**(I)**. Error bars represent binomial confidence interval with 95% significance.

Figure S9: L1210 synchronization using Baby Machine. A) Baby Machine synchronization. L1210 cells were released from the "Baby Machine" and were incubated for 0-9 hours after release. Cells were harvested, Stained with PI and scanned using flow cytometer. The fraction of cells at G1, S and G2 was determined. The experiment was repeated 4 times with similar results. **B) FACS analyses.** Shown are representative figures for 0, 3, 5, 7 and 9 hours after release from Baby Machine. We determined Early S as 3 hours, Mid S as 5 hours, and late S as 7 hours after release**.**

Figure S10: 3T3 synchronization using serum starvation. A) Serum starvation synchronization. BALB/3T3 cells were released from serum starvation and were incubated for 14-28 hours after release. Cells were harvested, Stained with DAPI and scanned using flow cytometer. The fraction of cells at G1, S and G2 were

determined. The experiment was repeated 2 times with similar results. **B) FACS analyses.** Shown are representative figures for 14, 18, 20, 22 and 26 hours after release from serum starvation. We determined Early S as 16-19 hours after release, Mid S as 20 hours, and late S as 22 hours after release.

1. Guelen, L., Pagie, L., Brasset, E., Meuleman, W., Faza, M.B., Talhout, W., Eussen, B.H., de Klein, A., Wessels, L., de Laat, W. *et al.* (2008) Domain organization of human chromosomes revealed by mapping of nuclear lamina interactions. *Nature*, **453**, 948-951.
2. Gaffney, D.J., McVicker, G., Pai, A.A., Fondufe-Mittendorf, Y.N., Lewellen, N., Michelini, K., Widom, J., Gilad, Y. and Pritchard, J.K. (2012) Controls of Nucleosome Positioning in the Human Genome. *Plos Genetics*, **8**.
3. Dixon, J.R., Selvaraj, S., Yue, F., Kim, A., Li, Y., Shen, Y., Hu, M., Liu, J.S. and Ren, B. (2012) Topological domains in mammalian genomes identified by analysis of chromatin interactions. *Nature*, **485**, 376-380.
4. Farkash-Amar, S., David, Y., Polten, A., Hezroni, H., Eldar, Y.C., Meshorer, E., Yakhini, Z. and Simon, I. (2012) Systematic determination of replication activity type highlights interconnections between replication, chromatin structure and nuclear localization. *PLoS One*, **7**, e48986.
5. Rivera-Mulia, J.C., Buckley, Q., Sasaki, T., Zimmerman, J., Didier, R.A., Nazor, K., Loring, J.F., Lian, Z., Weissman, S.M., Robins, A.J. *et al.* (2015) Dynamic changes in replication timing and gene expression during lineage specification of human pluripotent stem cells. *Genome Res*.

A

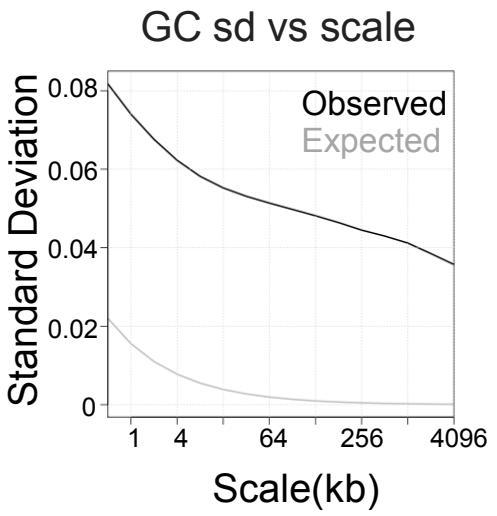

B

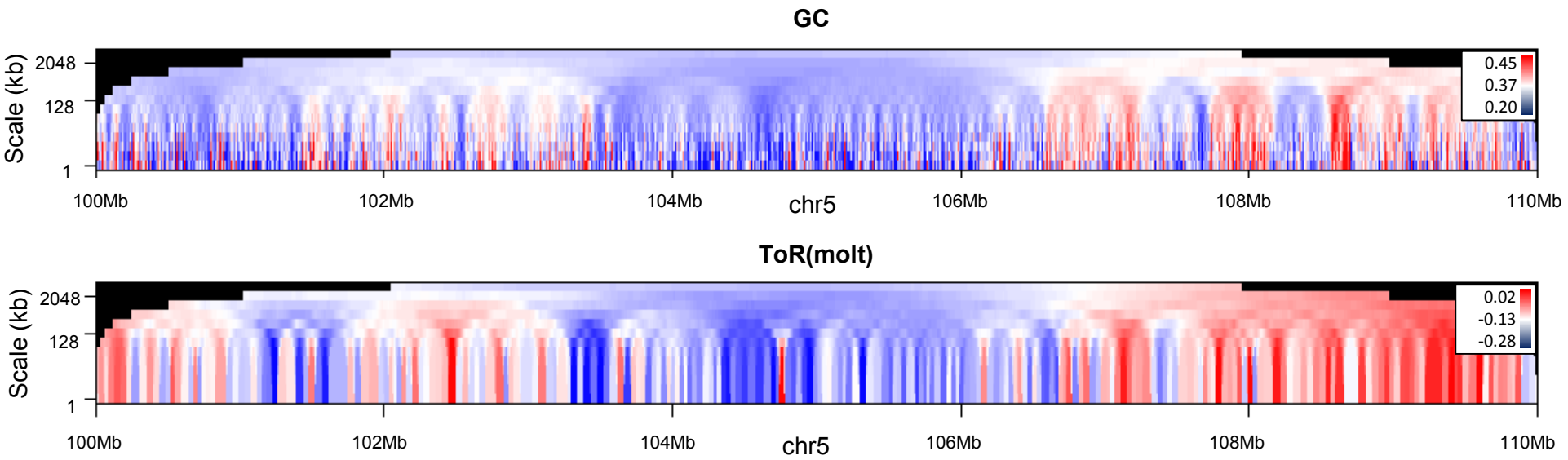

C

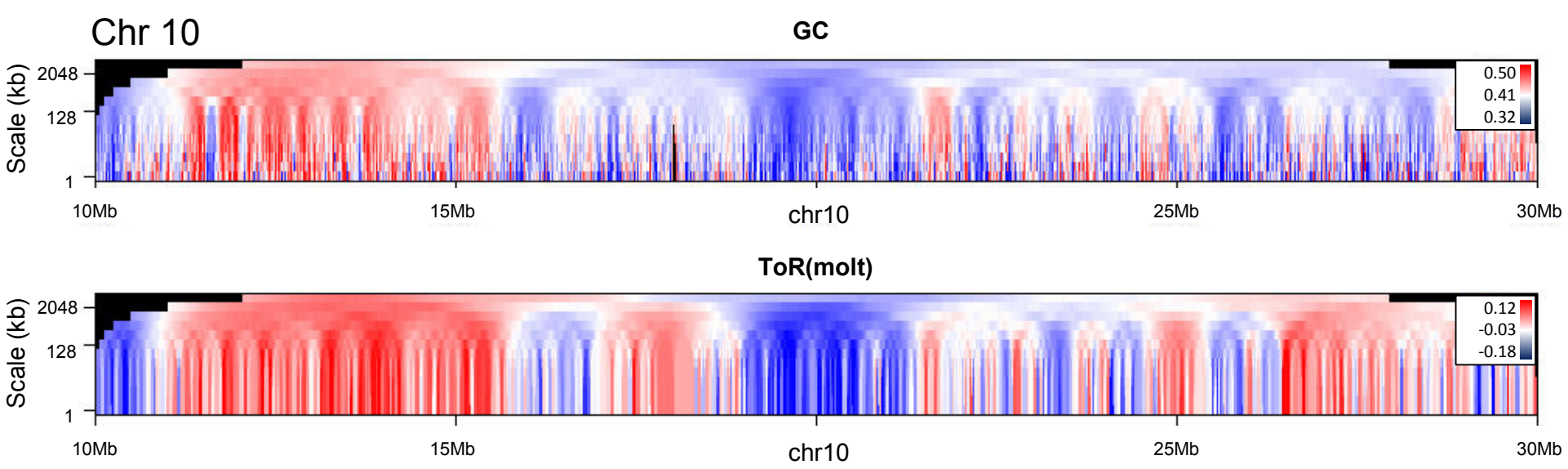

D

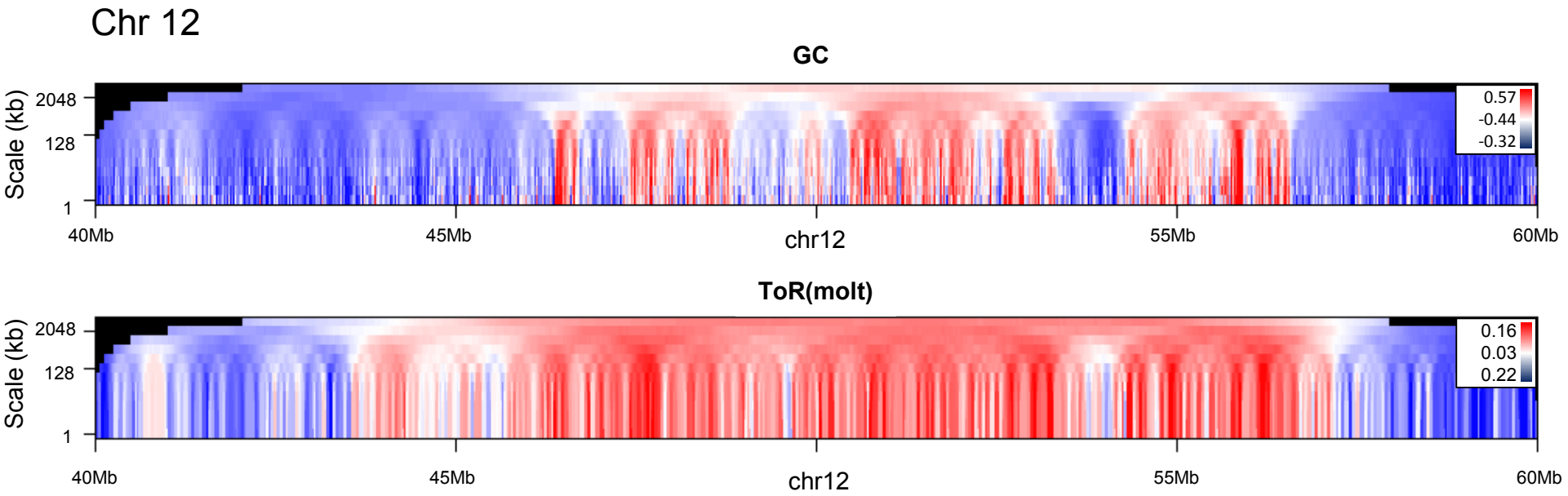

Figure s1

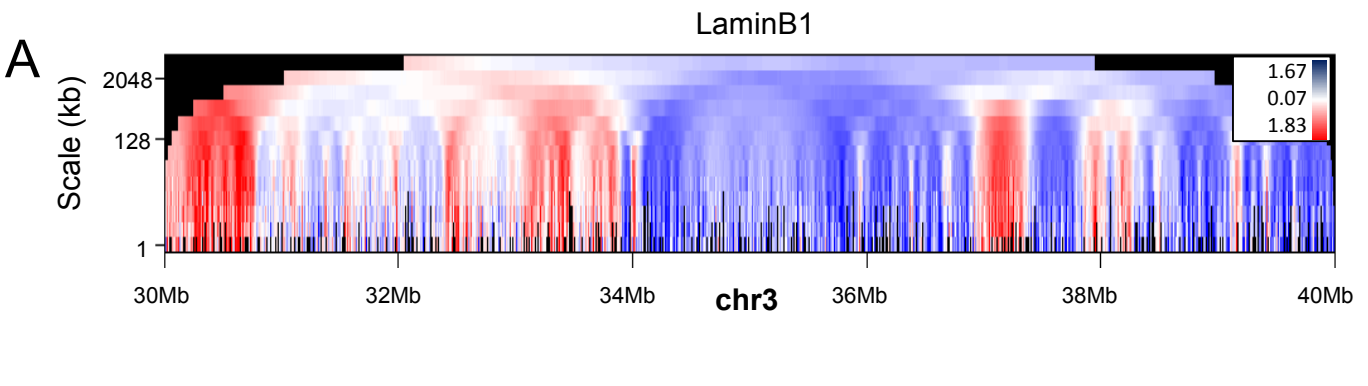
A
LaminB1
Scale (kb)
2048
128
1
1.67
0.07
1.83
30Mb
32Mb
34Mb
chr3
36Mb
38Mb
40Mb

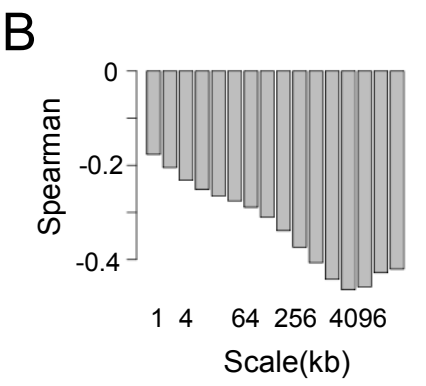
B
Spearman
0
-0.2
-0.4
1 4 64 256 4096
Scale(kb)

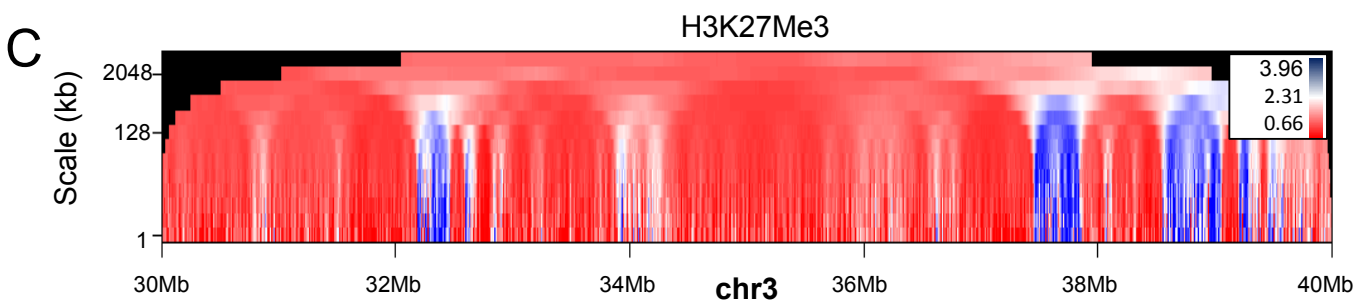
C
H3K27Me3
Scale (kb)
2048
128
1
3.96
2.31
0.66
30Mb
32Mb
34Mb
chr3
36Mb
38Mb
40Mb

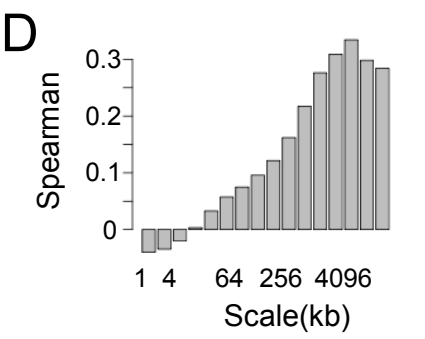
D
Spearman
0.3
0.2
0.1
0
1 4 64 256 4096
Scale(kb)

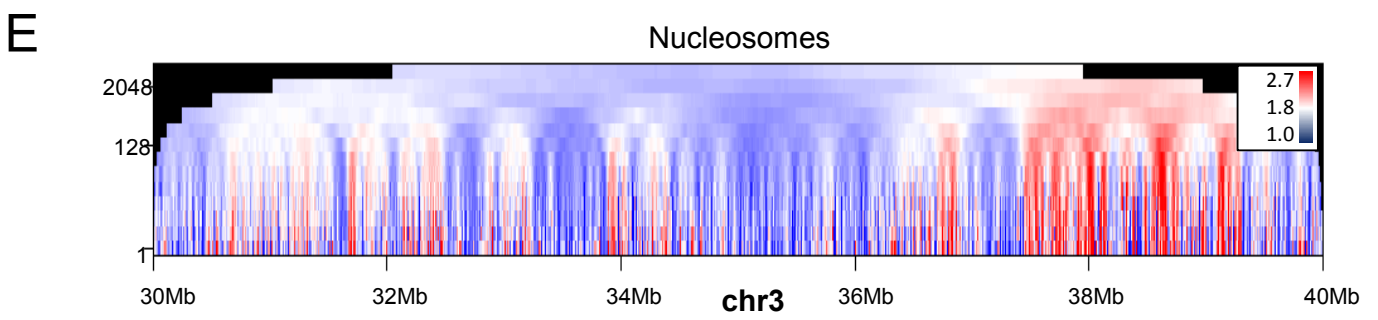
E
Nucleosomes
2048
128
1
2.7
1.8
1.0
30Mb
32Mb
34Mb
chr3
36Mb
38Mb
40Mb

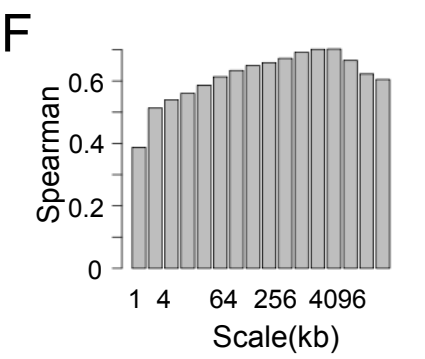
F
Spearman
0.6
0.4
0.2
0
1 4 64 256 4096
Scale(kb)

Figure s2

A

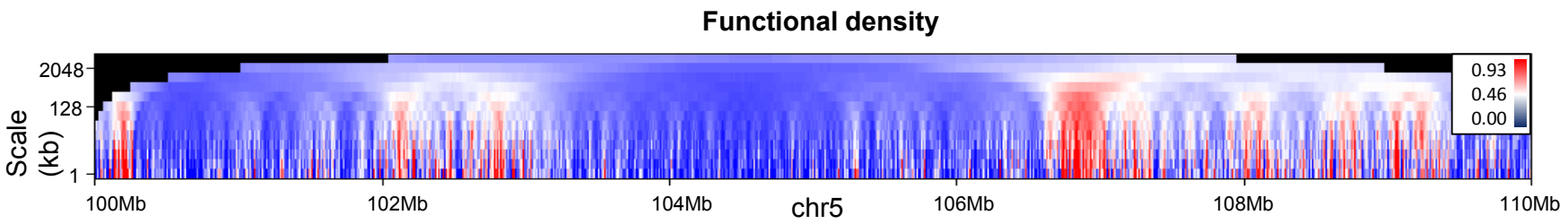

B

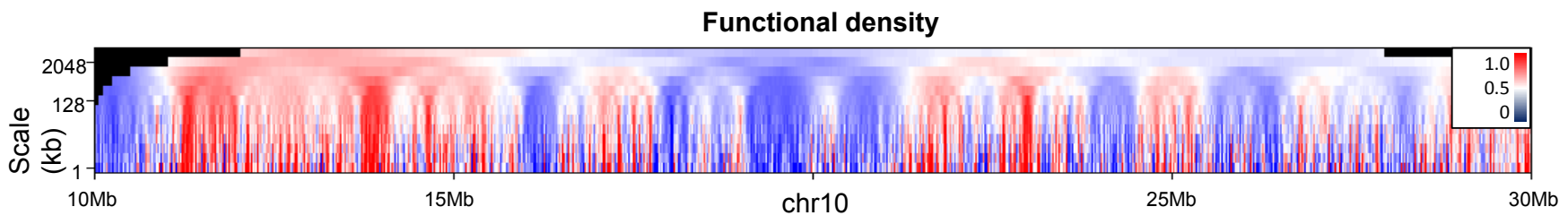

C

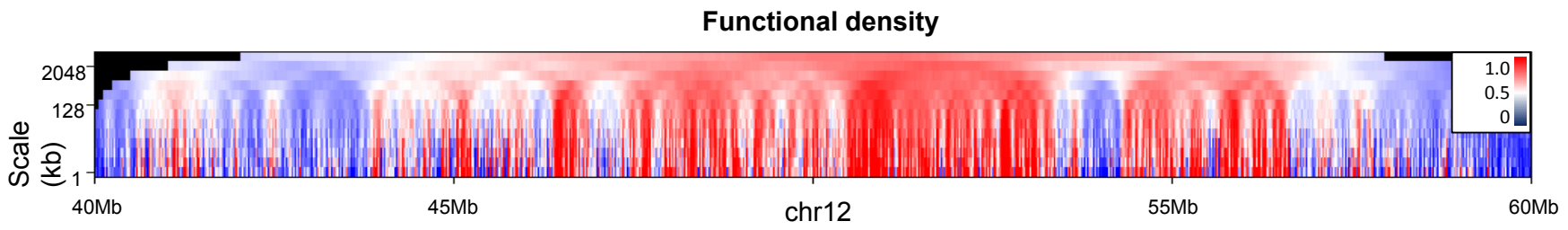

D

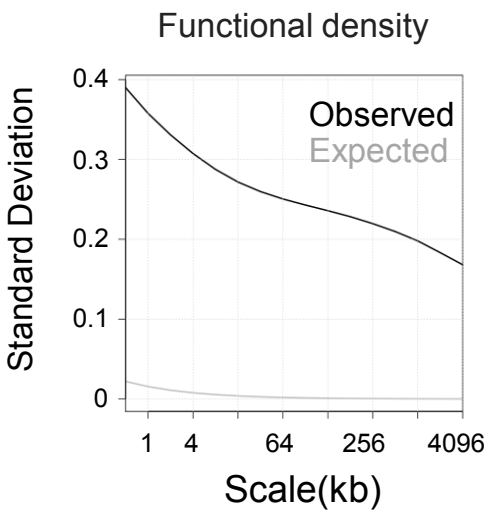

E

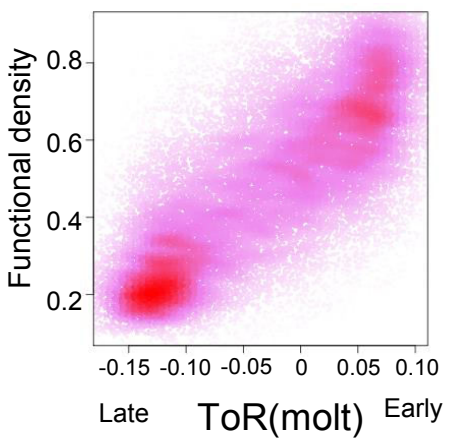

F

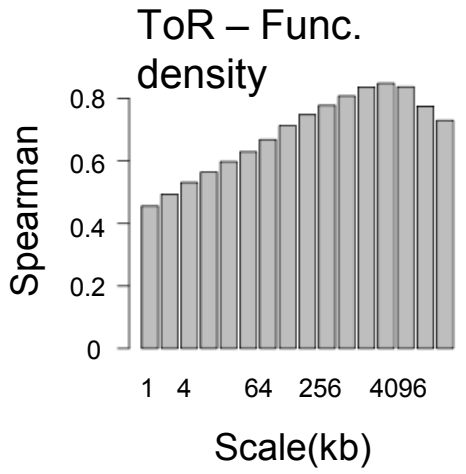

G

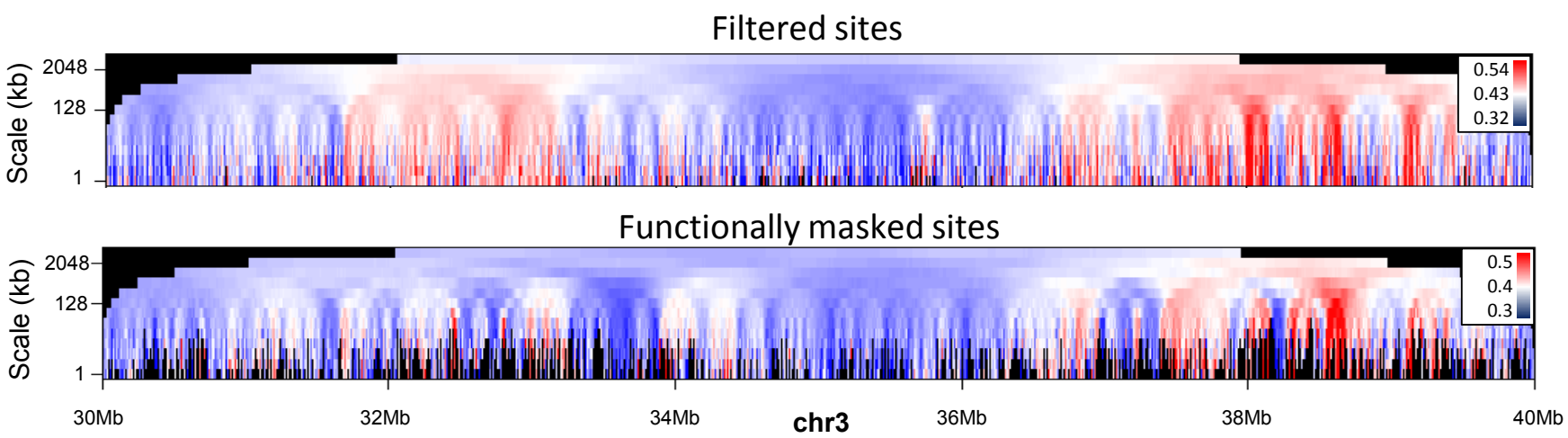

H

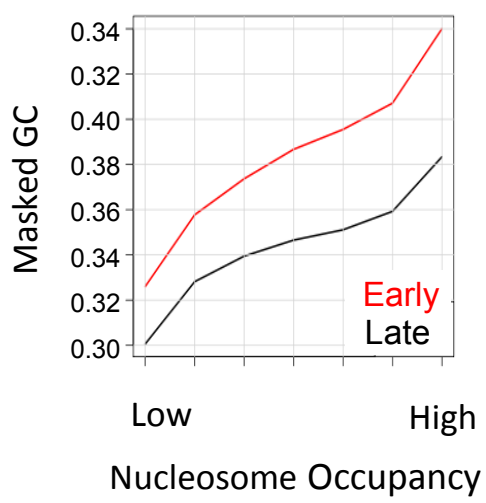

I

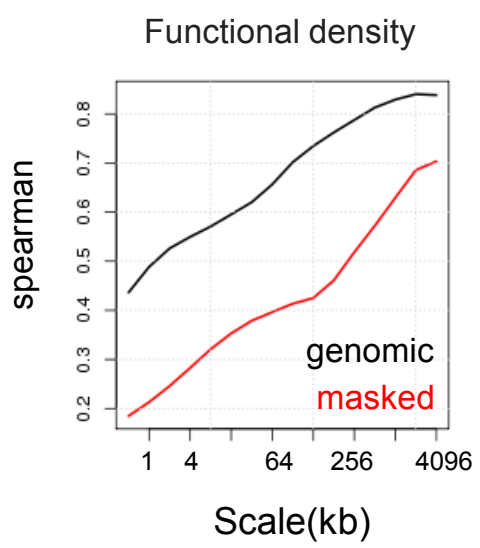

Figure s3

A

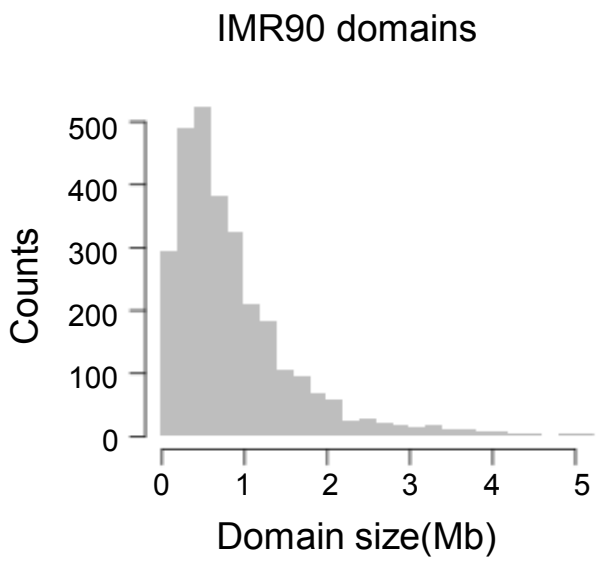
IMR90 domains
Counts
500
400
300
200
100
0
0
1
2
3
4
5
Domain size(Mb)

B

func dens
TOR(molt)
GC
p(AT->GC)
p(GC->AT)
10
7
3
5
4
9
0 2 7 11 16
Contact enrichment
IMR 90(Dixon et al.)

Figure s4

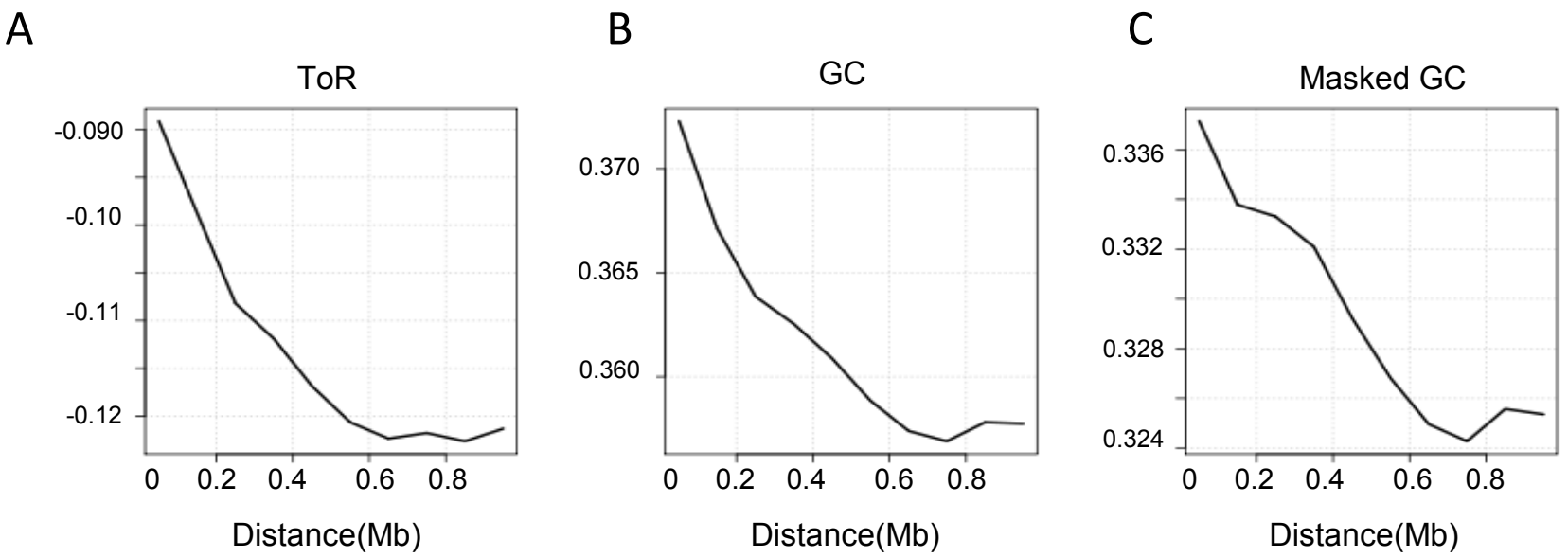
A
ToR
-0.090
-0.10
-0.11
-0.12
0
0.2
0.4
0.6
0.8
Distance(Mb)
B
GC
0.370
0.365
0.360
0
0.2
0.4
0.6
0.8
Distance(Mb)
C
Masked GC
0.336
0.332
0.328
0.324
0
0.2
0.4
0.6
0.8
Distance(Mb)
D
Functional Density
0.08
0.07
0.06
0.05
0
0.2
0.4
0.6
0.8
Distance(Mb)
E
LaminB1
0.50
0.45
0.40
0.35
0
0.2
0.4
0.6
0.8
Distance(Mb)
F
Scaling Factor
1.6
1.4
1.2
1.0
0
0.2
0.4
0.6
0.8
Distance(Mb)

Figure s5

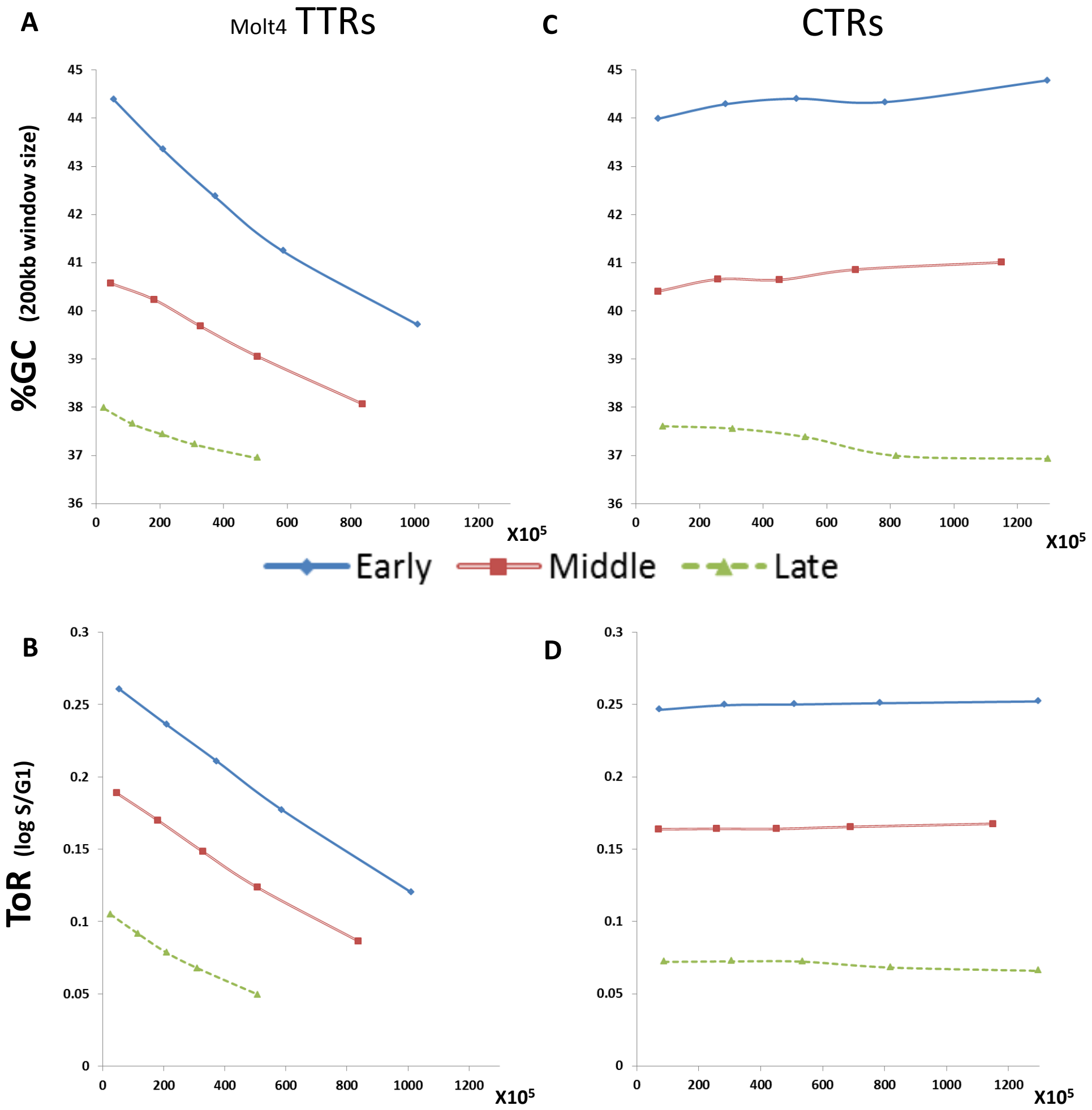
A
Molt4 TTRs
C
CTRs
%GC (200kb window size)
45
44
43
42
41
40
39
38
37
36
0
200
400
600
800
1000
1200
X10^5
Early
Middle
Late
B
D
ToR (log S/G1)
0.3
0.25
0.2
0.15
0.1
0.05
0
Distance from border of segment
Distance from border of segment

Figure s6

A

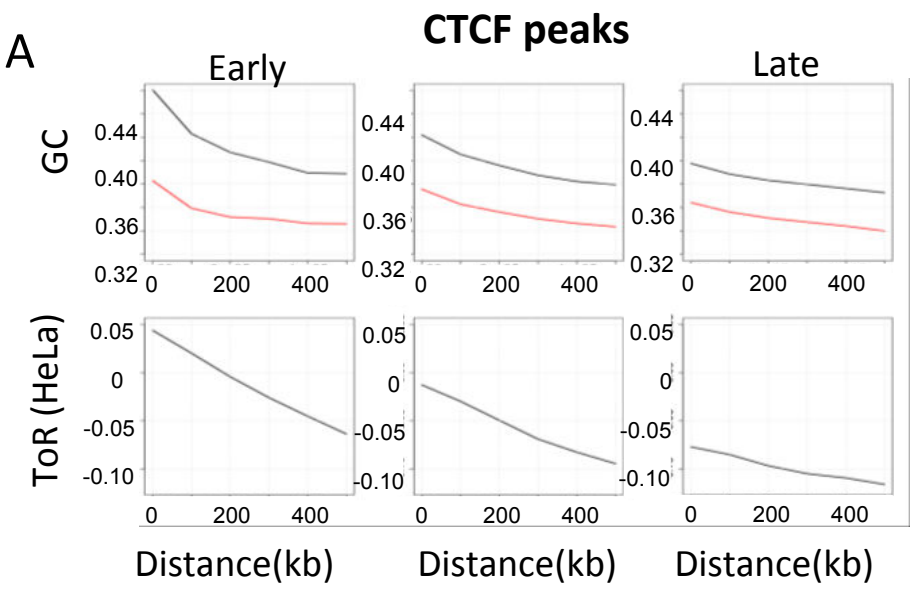

B

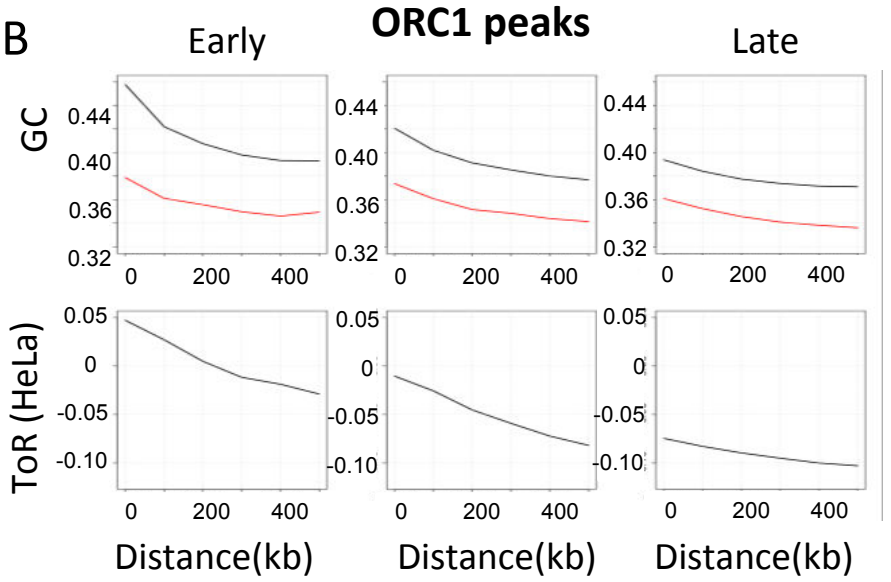

C

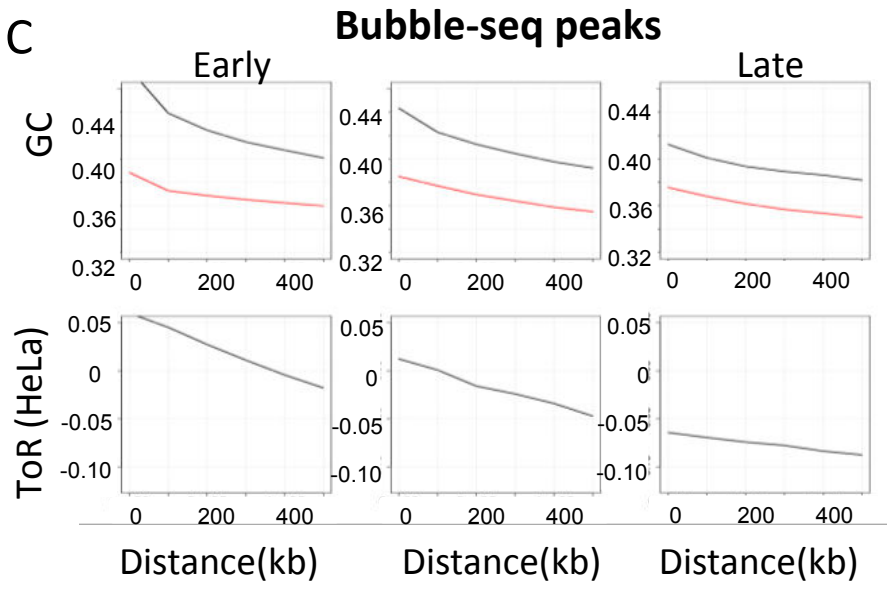

D

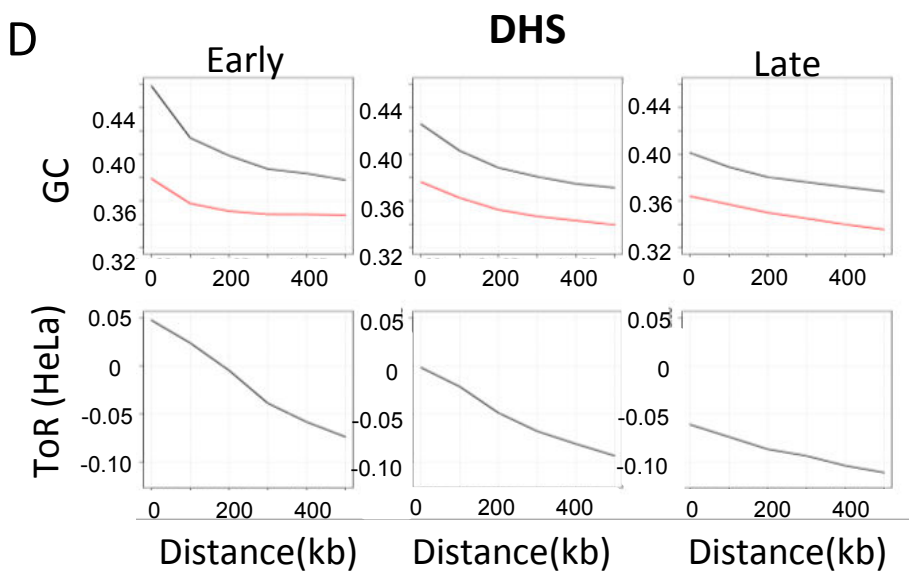

Figure s7

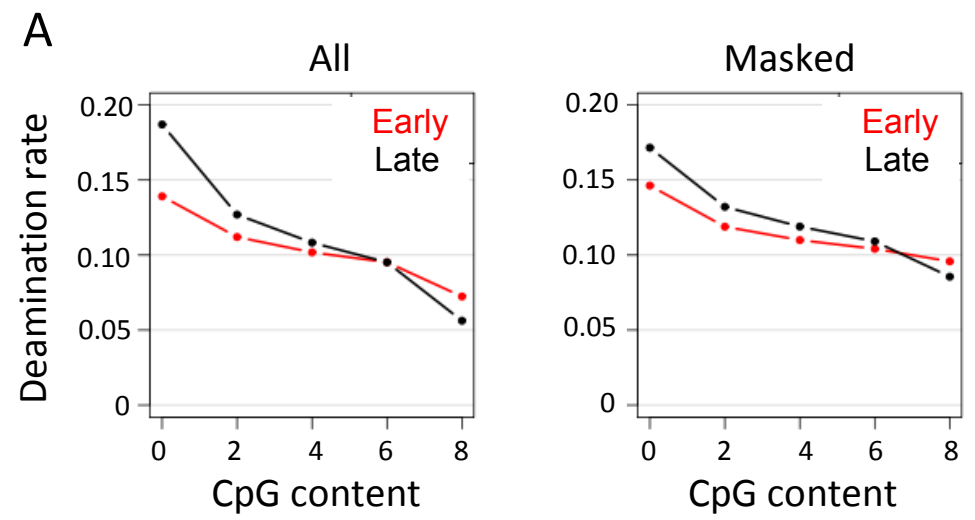
A
All
Masked
Deamination rate
Early
Late
CpG content

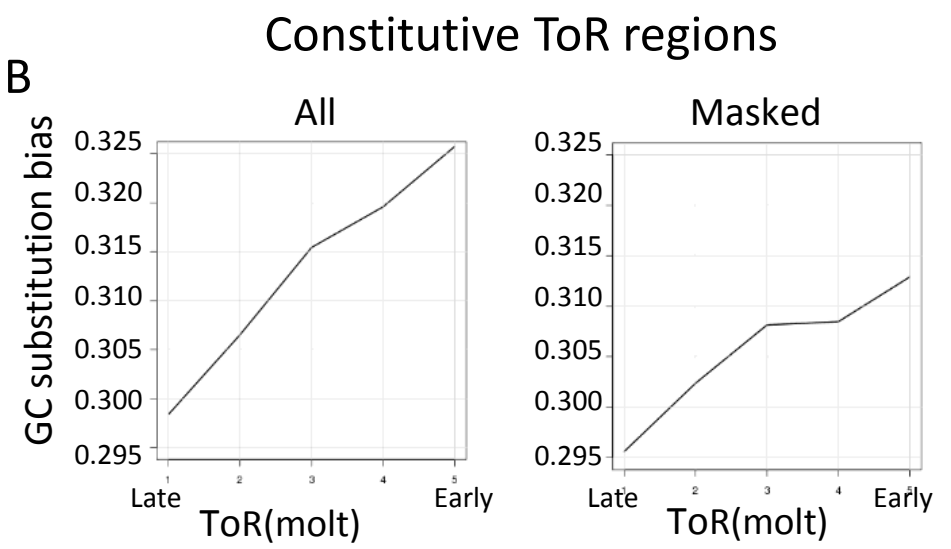
Constitutive ToR regions
B
All
Masked
GC substitution bias
Late
Early
ToR(molt)

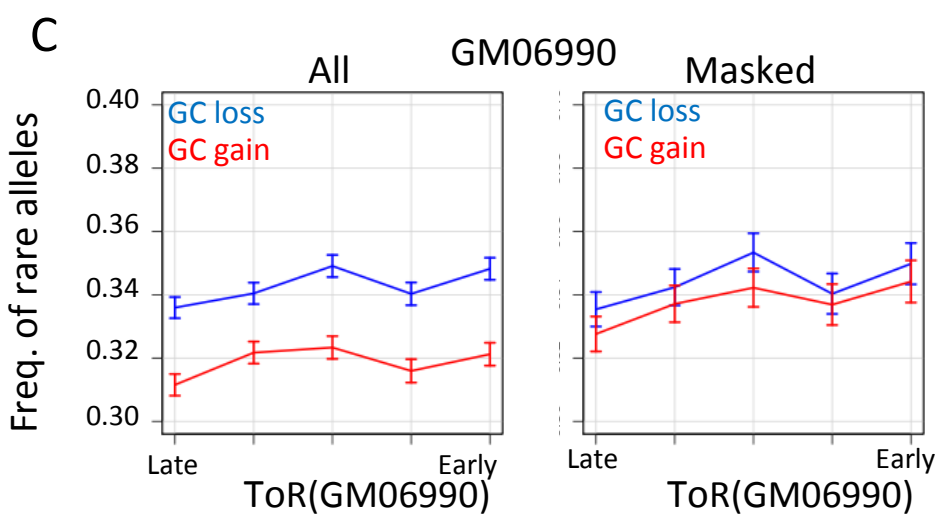
C
GM06990
All
Masked
Freq. of rare alleles
GC loss
GC gain
Late
Early
ToR(GM06990)

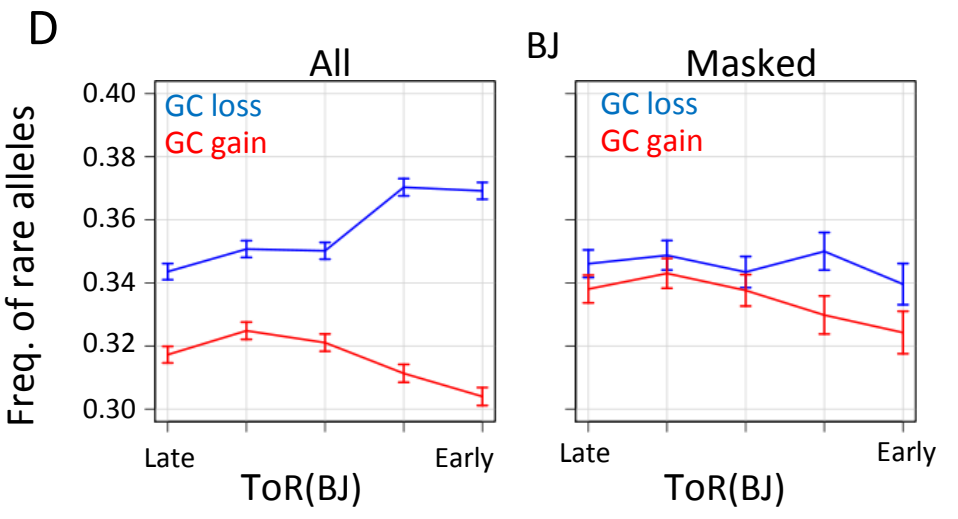
D
All
Masked
BJ
Freq. of rare alleles
GC loss
GC gain
Late
Early
ToR(BJ)

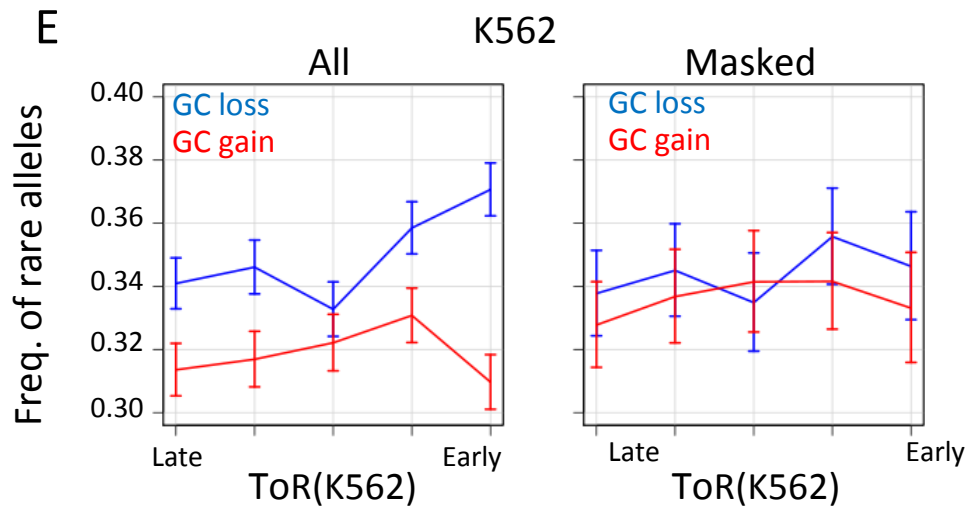
E
K562
All
Masked
Freq. of rare alleles
GC loss
GC gain
Late
Early
ToR(K562)

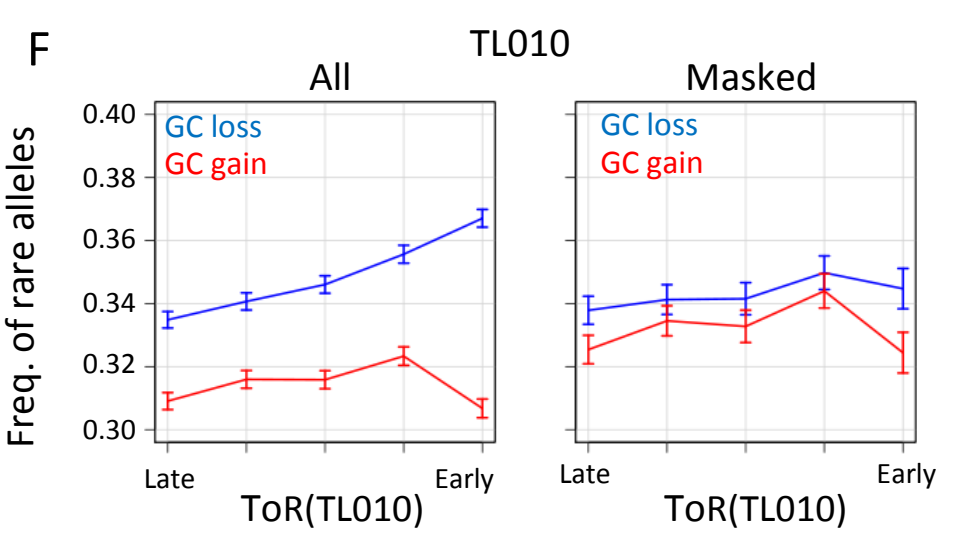
F
TL010
All
Masked
Freq. of rare alleles
GC loss
GC gain
Late
Early
ToR(TL010)

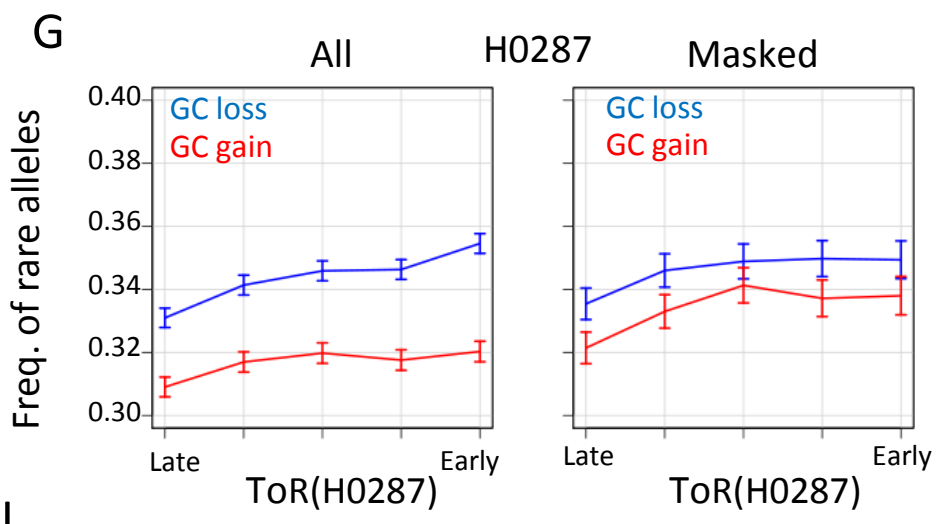
G
H0287
All
Masked
Freq. of rare alleles
GC loss
GC gain
Late
Early
ToR(H0287)

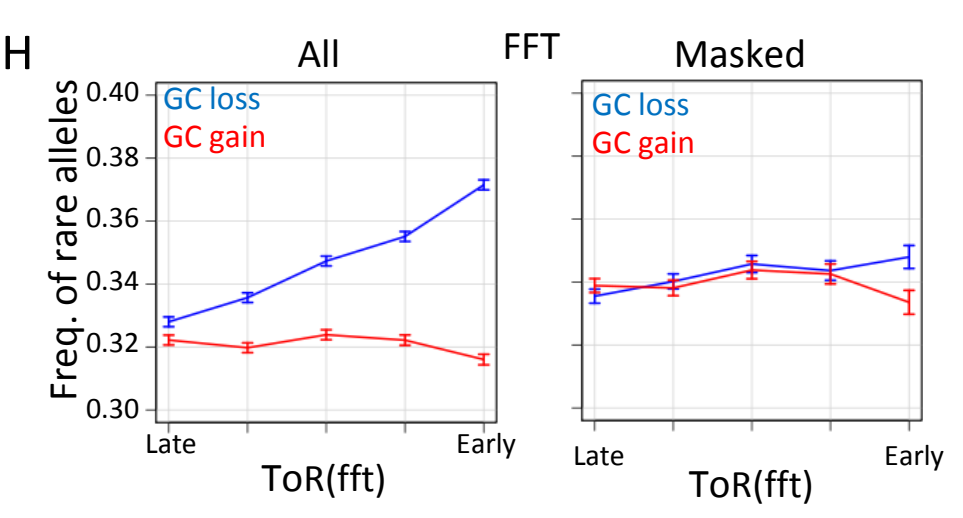
H
FFT
All
Masked
Freq. of rare alleles
GC loss
GC gain
Late
Early
ToR(fft)

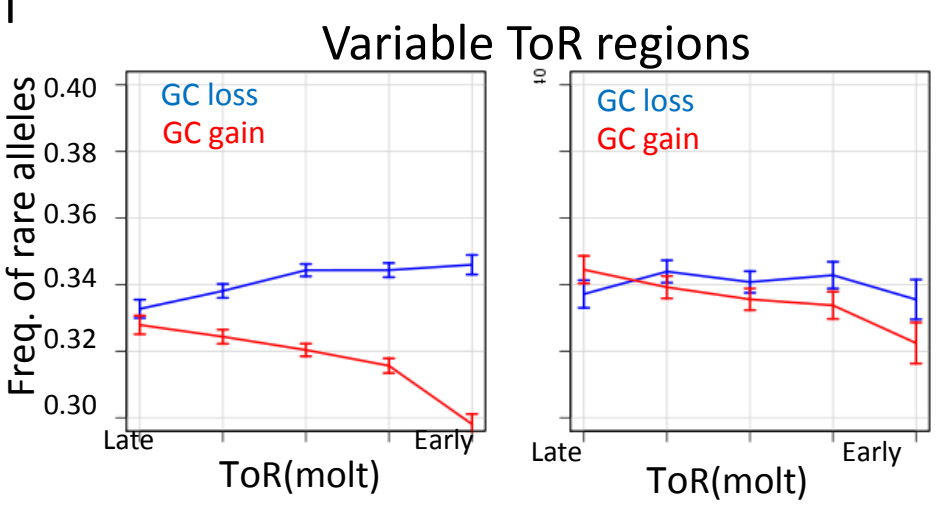
I
Variable ToR regions
Freq. of rare alleles
GC loss
GC gain
Late
Early
ToR(molt)

Figure s8

A

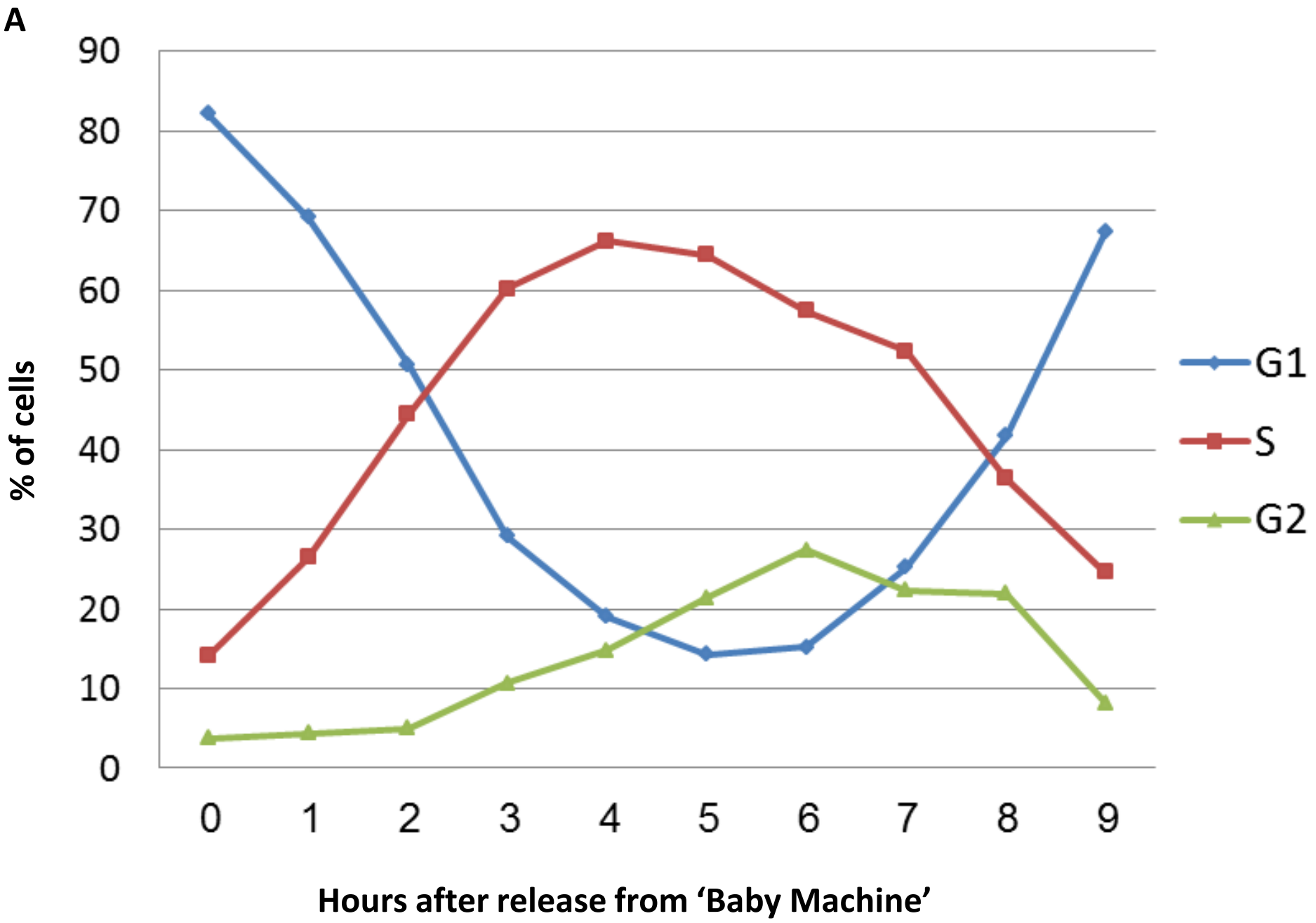
L1210 synchronization
% of cells
90
80
70
60
50
40
30
20
10
0
0
1
2
3
4
5
6
7
8
9
G1
S
G2
Hours after release from 'Baby Machine'

B

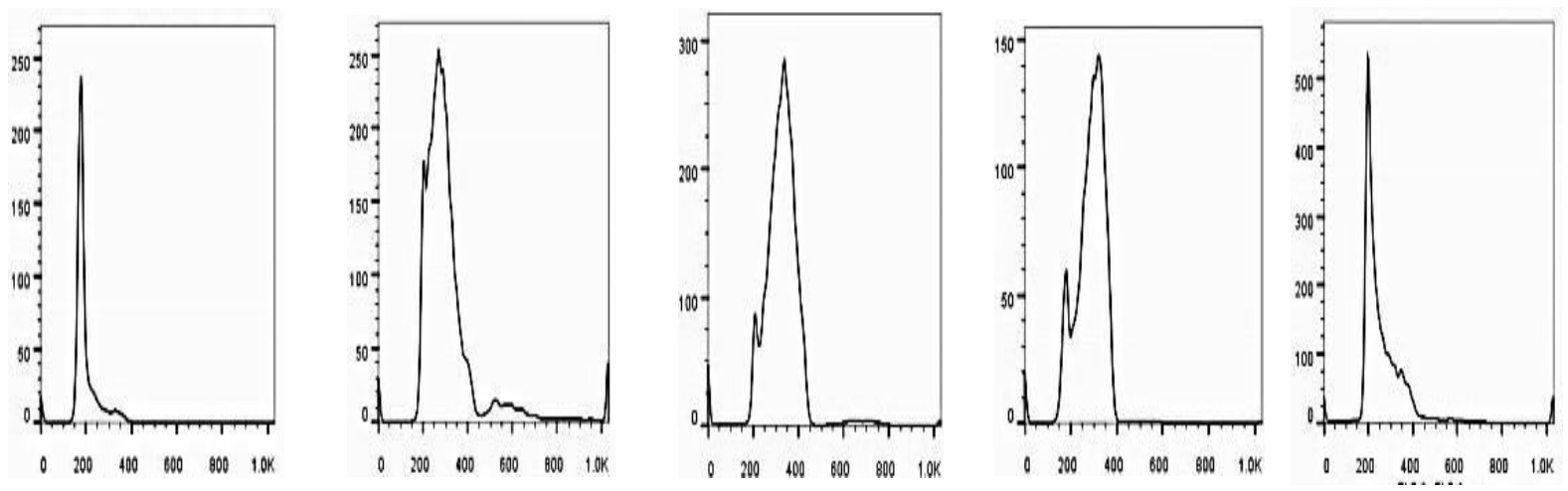
0
3
5
7
9
Hours after release from 'Baby Machine'

Figure s9

A

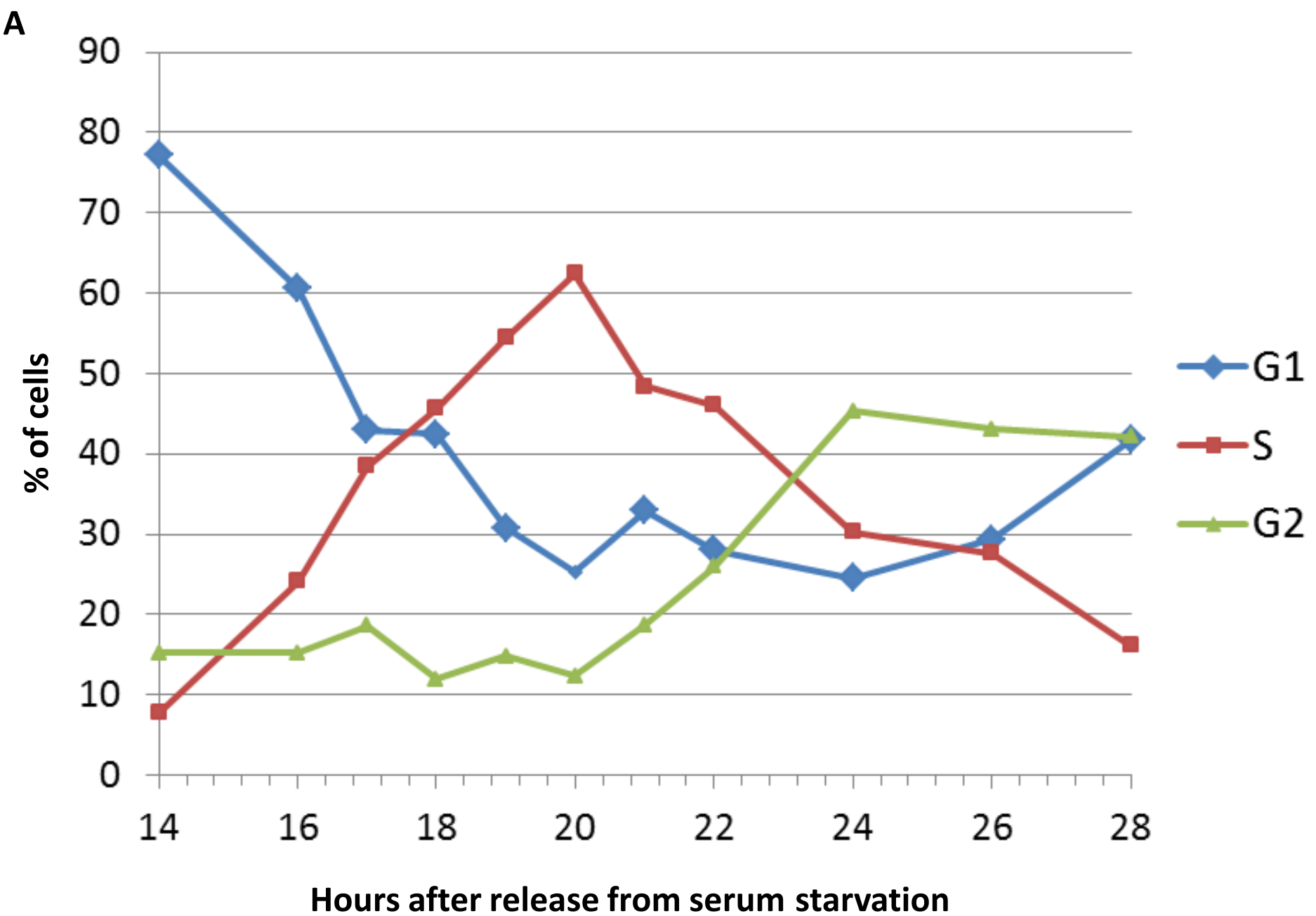

B

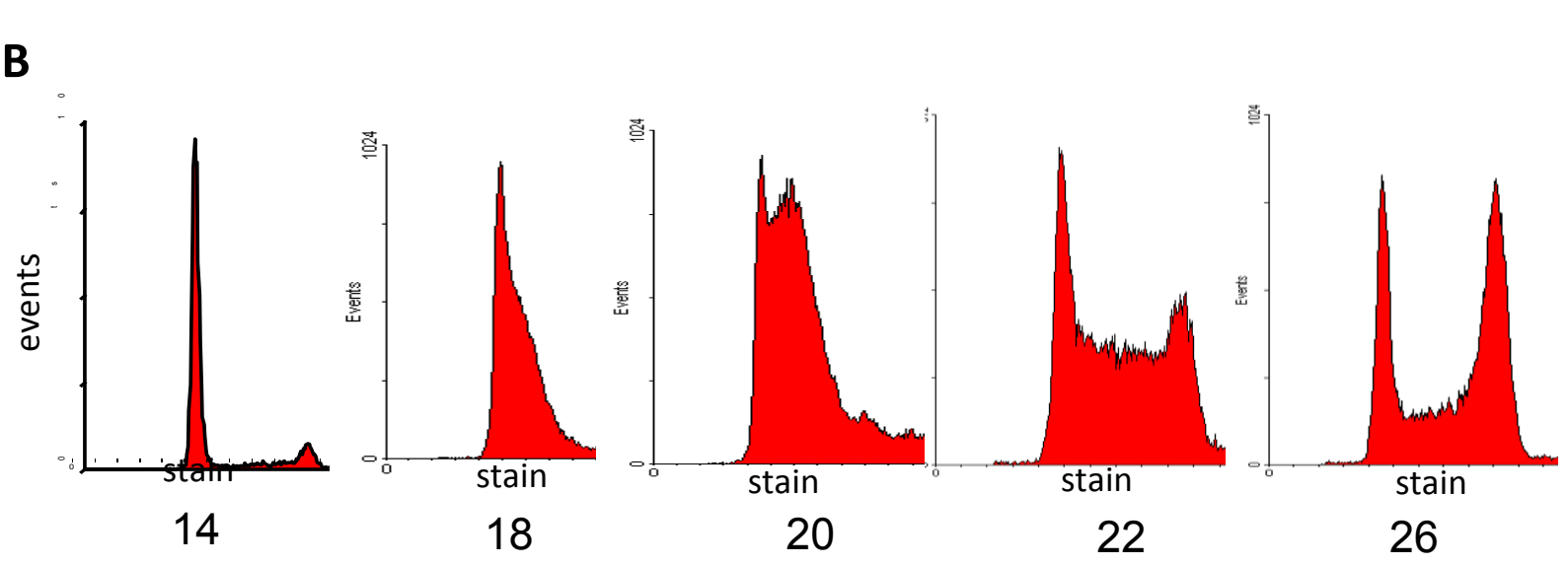

Figure s10